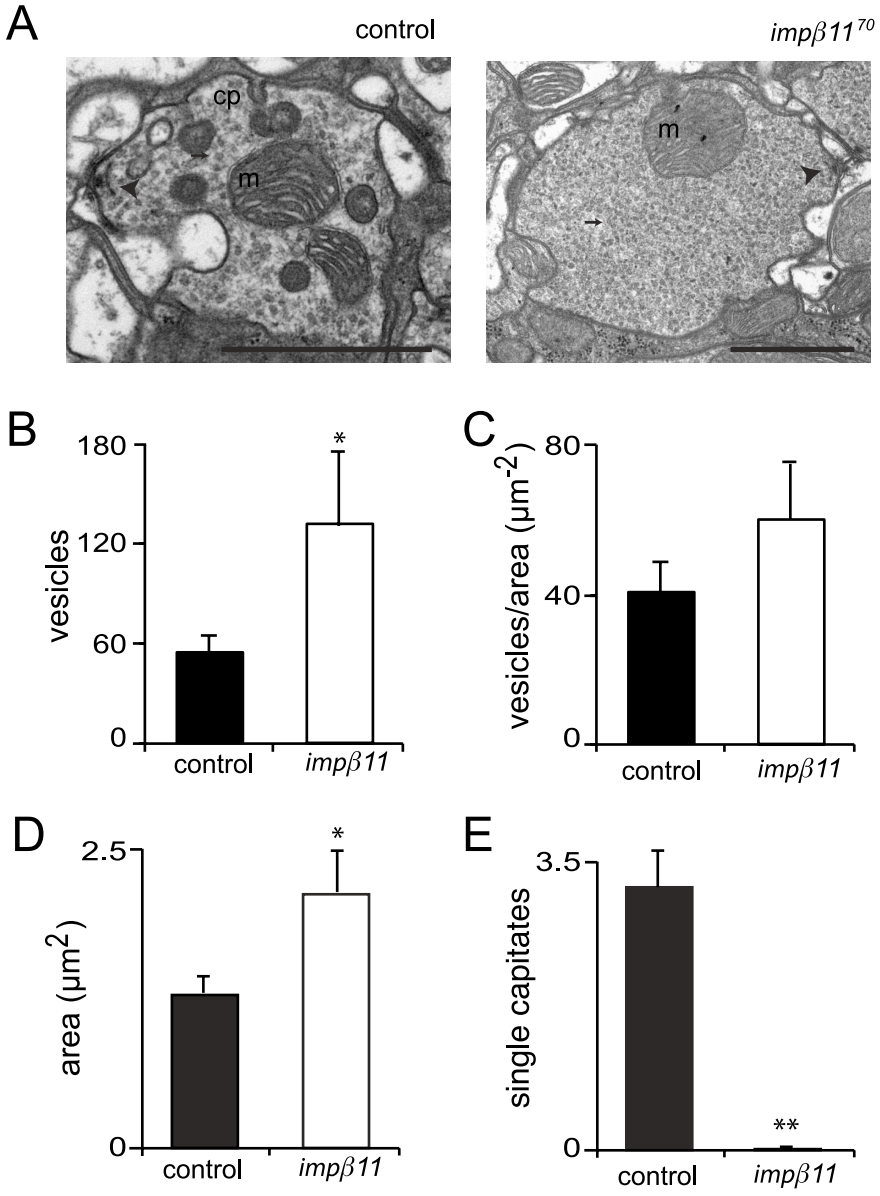

Supplemental Figure S1. *impβ11* photoreceptors contain excess synaptic vesicles.

(A) Representative electron micrographs of control (*y,w; FRT42D*) and *impβ11*^{70} (*y,w; FRT42D, impβ11*^{70}*/FRT42D, GMR-hid, cl; EGUF/+*) photoreceptor terminals. *Impβ11*^{70} terminals, like controls, contain T-bar densities at tetrad synapses (arrowheads), synaptic vesicles (arrows), and mitochondria (m), but profiles of capitate projections (cp) - invaginations into the terminal by surrounding glia - are rarely seen in *impβ11*^{70}. Scale bar = 1 μm. (B-D) The terminals of *impβ11*^{70} mutants have significantly more synaptic vesicles than control terminals but their packing density was unchanged because mutant terminals were significantly larger in profile area than control terminals. (E) Mutant terminals have few or no penetrating capitate projections. P values: *<0.05, **<0.001.

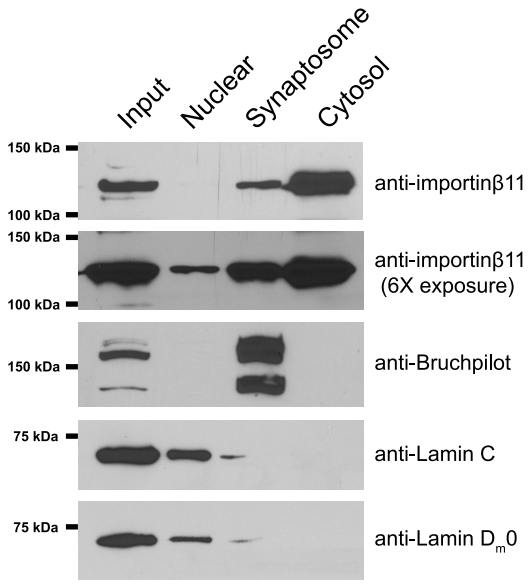

Supplemental Figure S2. Importin-β11 is Present in Synaptic, Cytosolic and Nuclear Fractions.

Subcellular fractionations of Drosophila heads were assessed on immunoblots for the presence of importin-β11. Importin-β11 was detected in synaptic, cytosolic and nuclear fractions. Detection in the nuclear contribution required a 6-fold longer exposure than the synaptic and cytosolic pools. The fractions were characterized with the synaptic marker Bruchpilot and nuclear markers Lamin C and Lamin D_m0. Each lane contains 1/500th of the final fraction volume.

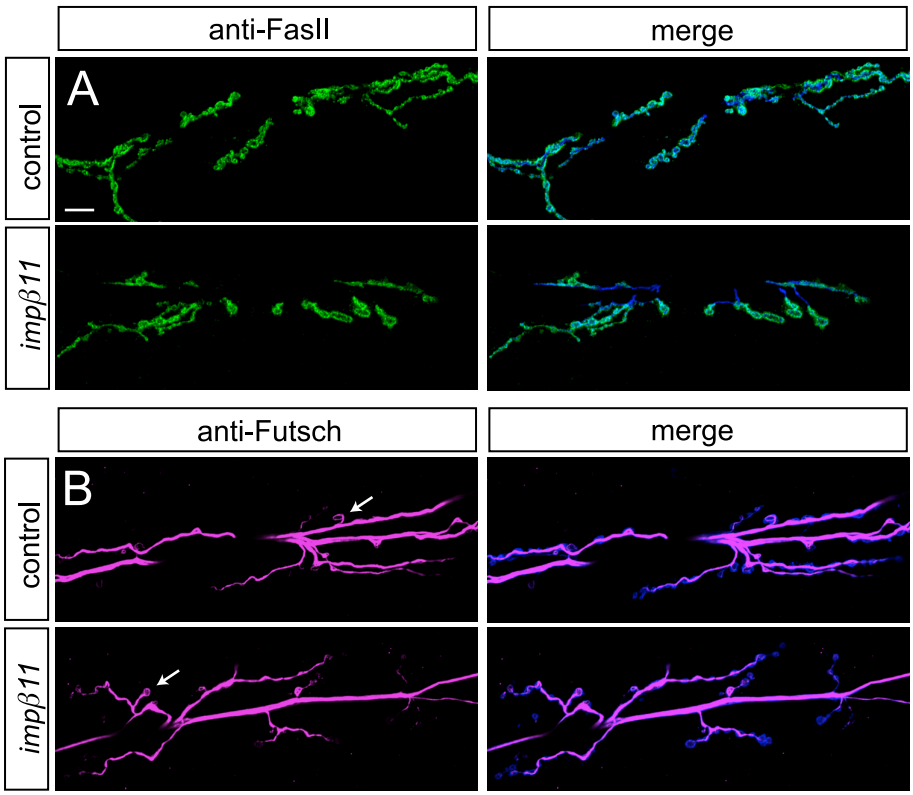

Supplemental Figure S3. FasII and Futsch localize to *impβ11* terminals.

Representative confocal immunolocalization of two proteins involved in NMJ development. Control (*y,w; FRT42D*) and *impβ11* (*FRT42D, impβ11^{70}/Df*) third-instar larvae were immunostained stained with anti-HRP (blue) and anti-FasII (A; green) or anti-Futsch (B; magenta). Localization and intensity were similar in control and mutant NMJs and both contained Futsch-immunoreactive loops of microtubules (arrows). Scale bar = 10μm.

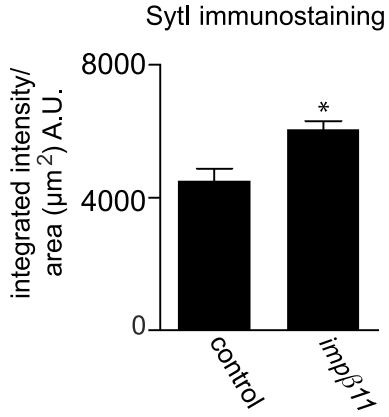

Supplemental Figure S4. Quantification of Anti-Syt I at the NMJ.

Immunoreactivity for the neuronal marker anti-HRP was used to generate regions of interest in control (*yw;FRT42D*) and *impβ11* (*FRT42D, impβ11^{70}/Df*) third-instar larvae. Integrated intensity within the region of interest was measured for anti-Syt I and divided by the area. Syt I levels in the mutant are moderately increased over those of control and therefore a loss of Syt I cannot account for the electrophysiological phenotypes. Error bars are mean ± SEM. P values: *<0.05 compared to control.

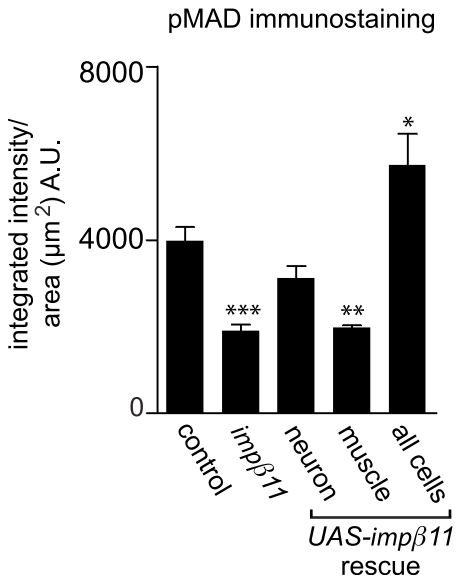

Supplemental Figure S5. Quantification of anti-pMAD immunoreactivity in *impβ11*.

The integrated fluorescence intensity of anti-pMAD immunostaining per μm^2 of the NMJ was significantly decreased in *impβ11* mutants. This reduction was rescued by neuronal but not muscle expression of *UAS-impβ11-eGFP*. Ubiquitous transgene expression raised pMAD to levels above those in control larvae but this may result from a difference in the strength of the driver rather than the site of expression. P values: *<0.05, **<0.001, ***<0.0001 compared to control.
Genotypes: control (*y,w;FRT42D*), *impβ11* (*FRT42D, impβ11^{70}/Df*), neuron (*FRT42D, impβ11^{70}/Df; elav-GAL4/UAS-impβ11-eGFP*), muscle (*FRT42D, impβ11^{70}, G14-GAL4/Df; UAS-impβ11-eGFP/+*), all cells (*FRT42D, impβ11^{70}/Df; da-GAL4/UAS-impβ11-eGFP*).

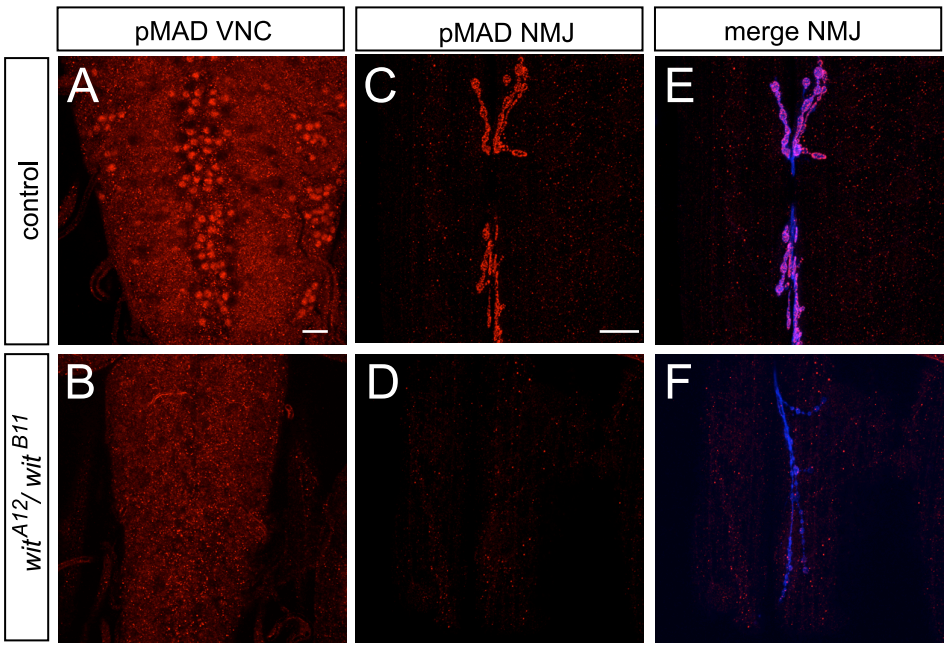

Supplemental Figure S6. pMAD immunoreactivity is absent from the VNC and NMJ of *wit* mutants.

Representative confocal images of VNCs and NMJs immunostained with anti-pMAD (red). (A,B) pMAD localizes to nuclei in the VNC in *y,w; FRT42D* animals, but is absent when the type II receptor *wit* is mutated, as previously reported (Marques et al., 2002). (C-F) At motor nerve terminals stained with anti-HRP (blue), pMad immunoreactivity is absent in *wit* mutants and thus the synaptic pMAD at the NMJ is dependent on Wit activation. Scale bar = 20μm.

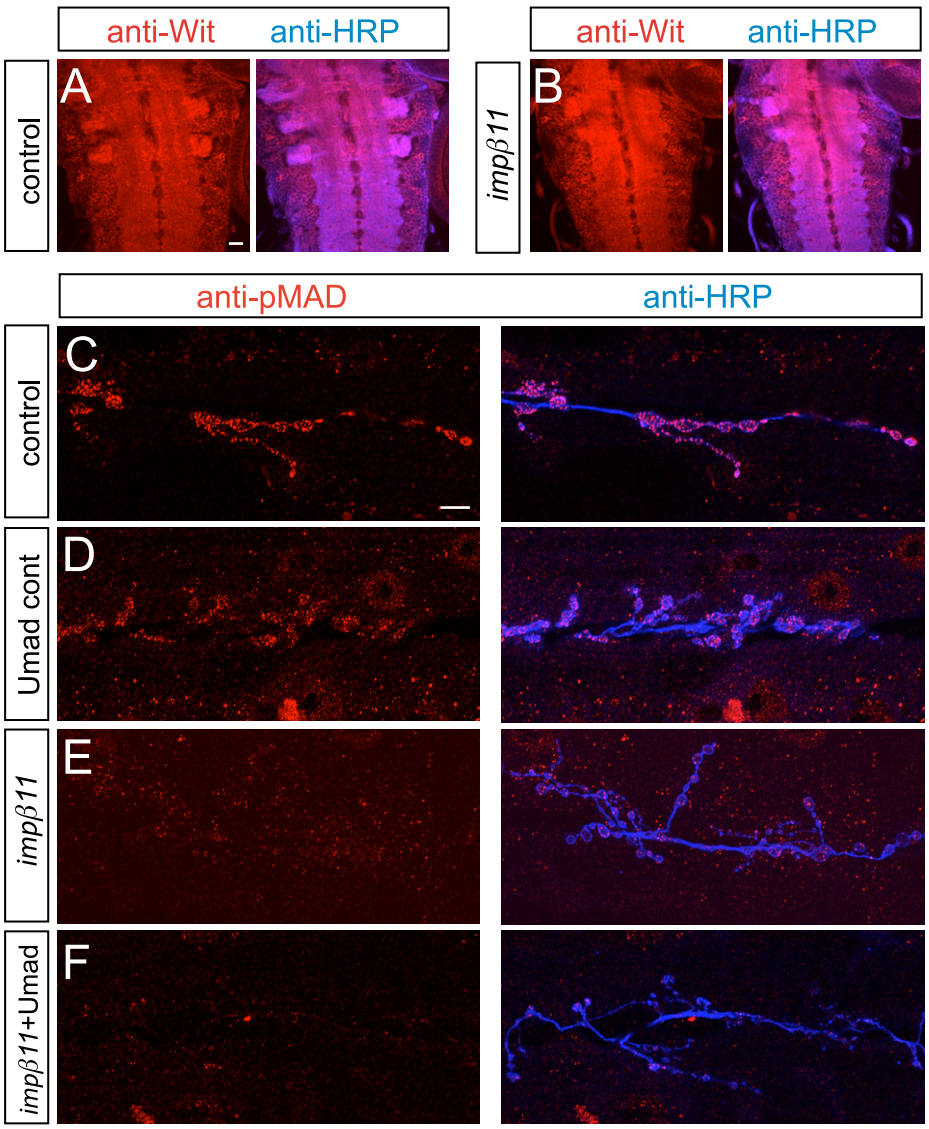

Supplemental Figure S7. Lack of Wit and MAD expression do not account for the loss of pMAD at *impβ11* NMJs.

(A,B) Anti-wit immunoreactivity (red) was present in *impβ11* VNCs suggesting that loss of Wit expression was not responsible for the reduced pMAD at *impβ11* synapses. (C-F) Synapses co-stained with anti-pMAD (red) and anti-HRP (blue). Expression of a *UAS-GFP-MAD* transgene in the nervous system did not significantly alter the localization or intensity of pMAD immunoreactivity in control larvae (D) or restore pMAD to *impβ11* mutant NMJs (F). Scale bars = 10μm.
Genotypes: control (*y,w; FRT42D*), Umad cont (e*lav-GAL4/UAS-GFP-MAD*), *impβ11*(*w;FRT42D, impβ11*^{70}*/Df*), *impβ11*+Umad (*w;FRT42D, impβ11*^{70}*/Df; elav-GAL4/UAS-GFP-MAD*).

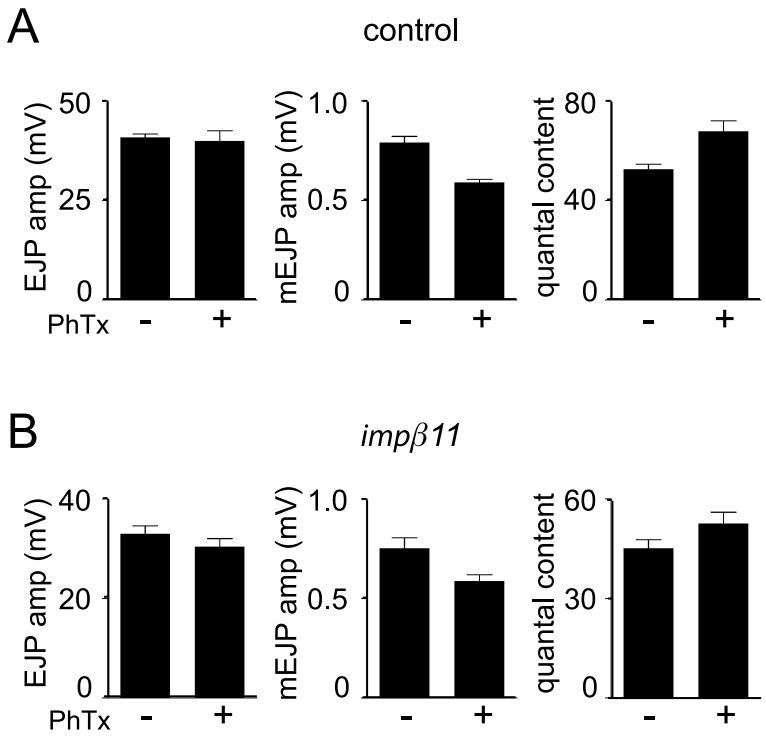

Supplemental Figure S8. PhTx-induced synaptic homeostasis persists in *impβ11* mutants.

Recordings from third-instar muscles in the absence (-) and presence (+) of 4 μM PhTx in 1 mM Ca^{2+} HL3 saline. (A) Due to homeostatic compensation, *y,w; FRT42D* larvae treated with PhTx had normal EJP amplitudes when compared to mock treated larvae despite reduced mEJP amplitudes. Quantal content was therefore increased by PhTx. Quantal content was also increased by PhTx exposure in *impβ11* mutant larvae (*y,w; FRT42D, impβ11^{70}/Df*). $n \geq 8$ for each genotype.